HAL
open science

End of a black hole's evaporation. II.

Farshid Soltani, Carlo Rovelli, Pierre Martin-Dussaud

To cite this version:

Farshid Soltani, Carlo Rovelli, Pierre Martin-Dussaud. End of a black hole's evaporation. II.. Phys.Rev.D, 2021, 104 (6), pp.066015. 10.1103/PhysRevD.104.066015 . hal-03239625

HAL Id: hal-03239625

https://hal.science/hal-03239625v1

Submitted on 2 Feb 2024

HAL is a multi-disciplinary open access archive for the deposit and dissemination of scientific research documents, whether they are published or not. The documents may come from teaching and research institutions in France or abroad, or from public or private research centers.

L'archive ouverte pluridisciplinaire **HAL**, est destinée au dépôt et à la diffusion de documents scientifiques de niveau recherche, publiés ou non, émanant des établissements d'enseignement et de recherche français ou étrangers, des laboratoires publics ou privés.

End of a black hole's evaporation. II.

Farshid Soltani,[1,2] Carlo Rovelli,[3,4,5] and Pierre Martin-Dussaud[6]

[1]*Department of Physics and Astronomy, University of Western Ontario, London, Ontario N6A 3K7, Canada*
[2]*Dipartimento di Fisica, Sapienza Università di Roma, P.le Aldo Moro 5, I-00185 Roma, Italy, EU*
[3]*AMU Université, Université de Toulon, CNRS, CPT, F-13288 Marseille, France, EU*
[4]*Perimeter Institute, 31 Caroline Street N, Waterloo, Ontario N2L2Y5, Canada*
[5]*The Rotman Institute of Philosophy, 1151 Richmond Street N, London N6A5B7, Canada*
[6]*Institute for Gravitation and the Cosmos, The Pennsylvania State University, University Park, Pennsylvania 16802, USA*

(Received 3 August 2021; accepted 5 August 2021; published 14 September 2021)

We derive an explicit expression for the transition amplitude from black to white hole horizon at the end of Hawking evaporation using covariant loop quantum gravity.

DOI: 10.1103/PhysRevD.104.066015

I. INTRODUCTION

The existence of a classical solution of the Einstein field equations describing a spacetime in which the exterior of a past black hole and a future white hole are connected [1] indicates that the end of the evaporation of a black hole can result in a quantum tunneling from a trapped to an antitrapped region. The black to white hole transition is receiving increasing attention in the literature [2–14]. In [15], following the scenario developed in [16–25], we have introduced a technique to study this transition. Here we use this technique to derive an explicit expression for the corresponding transition amplitude.

This transition amplitude is formally given by a path integral over four geometries performed on a spacetime region B bounded by a three-dimensional surface Σ (with specified intrinsic and extrinsic geometry). The three-dimensional surface Σ encloses the transition region. Its specification and its geometry have been computed in [15]. The formal path integral is approximated and concretely defined by the spin foam amplitude [26] associated to a discretization of B. While the discretization of Σ was defined in [15], here we construct the full discretization of B and compute the corresponding transition amplitude.

The complexity of the calculation is given by the topology of B, which is the product of a two-sphere and a disk (see Fig. 1). The disk is the product of a finite time interval and a finite space (radial) interval and it is delimited by an exterior two-sphere S_+ that surrounds the horizon and by an interior two-sphere S_- surrounded by the horizon (sitting on the bounce radius of the transition of the internal geometry of the black hole). The two two-spheres S_+ and S_- split Σ into a past component Σ^p and a future component Σ^f.

While Σ was discretized by means of a three-dimensional triangulation, here we discretize B in terms of a two-complex $\mathcal{C}$ dual to a cellular complex which is not a four-dimensional triangulation. This choice has the advantage of providing a relatively simple discretization that respects the symmetries of the problem.

Section II is devoted to the construction of the two-complex $\mathcal{C}$. The corresponding transition amplitude is computed in Sec. III. Section IV offers a simplification of the expression based on the symmetries of the two-complex. Section V gives the amplitude in terms of coherent states. The duals of Γ and $\mathcal{C}$, namely the triangulation of Σ and the cellular decomposition of B, are discussed in Appendix A. Appendix B offers a graphical representation of Γ and $\mathcal{C}$. Appendix C recalls the basic formulas of covariant loop quantum gravity.

II. DISCRETIZATION OF *B*

In this section we give the combinatorial definition of the two-complex $\mathcal{C}$ as a set of vertices, edges and faces with their boundary relations. To help the geometric visualization, a graphical representation of the two-complex $\mathcal{C}$ and its boundary Γ is provided in Appendix B: we advise the reader to consult it.

If N_1 and N_2 are nodes, we write $\mathrm{L} = (\mathrm{N}_1, \mathrm{N}_2)$ to denote the oriented link with source N_1 and target N_2. We denote $\mathrm{L}^{-1} \equiv (\mathrm{N}_2, \mathrm{N}_1)$ the same link but with opposite orientation. For the vertices and edges of the two-complex of the spin foam (which form a graph), we use an analogous notation. We denote the vertices as v; the internal edges (bounded by two vertices) as e; the external edges (bounded by one node) as E. Similarly, we denote the internal faces (bounded by internal edges only) as f; the external faces (with one link in the boundary) as F. We write $\mathrm{f} = (\mathrm{e}_1, \ldots, \mathrm{e}_n)$ to denote the oriented face f bounded by these edges. The orientation of the face is given by the sequence

 © 2021 American Physical Society

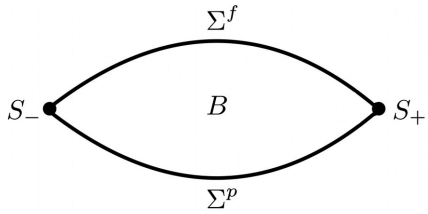

FIG. 1. The region B in the time-radius space: each point of the diagram is a two-sphere.

of edges. These are written oriented accordingly to the orientation the face induces on them.

Let a, b, c, d be indices taking values in the set $\{1,2,3,4\}$, t be an index taking values in the set $\{p,f\}$ (for past and future) and ϵ be an index taking values in the set $\{-,+\}$ (for interior and exterior). In all the expressions with several indices $a,b,\ldots$ these are assumed to be all different, that is $a \neq b$ and so on. Unless two indices are separated by a comma, the order of the indices is not relevant and exchanging the indices results in the same element. If two indices are separated by a comma, exchanging the indices results in a different element.

The graph Γ dual to the three-dimensional triangulation of Σ constructed in [15] is defined by

Nodes $\mathrm{N}_a^{t\epsilon}$ and N_{ab}^t;

Links $\mathrm{L}_a^\epsilon = (\mathrm{N}_a^{p\epsilon}, \mathrm{N}_a^{f\epsilon})$,
$\mathrm{L}_{a,b}^{t+} = (\mathrm{N}_{ab}^t, \mathrm{N}_a^{t+})$,
$\mathrm{L}_{a,b}^{t-} = (\mathrm{N}_{cd}^t, \mathrm{N}_a^{t-})$.

(See Fig. 6 of Appendix B.)

The two-complex $\mathcal{C}$, whose boundary $\partial\mathcal{C}$ is given by Γ, is defined by

Vertices v_a^ϵ and v_{ab};

Edges $\mathrm{E}_a^{t\epsilon} = (\mathrm{v}_a^\epsilon, \mathrm{N}_a^{t\epsilon})$,
$\mathrm{E}_{ab}^t = (\mathrm{v}_{ab}, \mathrm{N}_{ab}^t)$,
$\mathrm{e}_{a,b}^+ = (\mathrm{v}_a^+, \mathrm{v}_{ab})$,
$\mathrm{e}_{a,b}^- = (\mathrm{v}_a^-, \mathrm{v}_{cd})$;

Faces $\mathrm{F}_a^\epsilon = (\mathrm{L}_a^\epsilon, (\mathrm{E}_a^{f\epsilon})^{-1}, \mathrm{E}_a^{p\epsilon})$,
$\mathrm{F}_{a,b}^{t+} = (\mathrm{L}_{a,b}^{t+}, (\mathrm{E}_a^{t+})^{-1}, \mathrm{e}_{a,b}^+, \mathrm{E}_{ab}^t)$,
$\mathrm{F}_{a,b}^{t-} = (\mathrm{L}_{a,b}^{t-}, (\mathrm{E}_a^{t-})^{-1}, \mathrm{e}_{a,b}^-, \mathrm{E}_{cd}^t)$,
$\mathrm{f}_{a,b} \overset{c<d}{=} (\mathrm{e}_{a,c}^+, (\mathrm{e}_{b,d}^-)^{-1}, \mathrm{e}_{b,c}^-, (\mathrm{e}_{a,d}^+)^{-1})$.

This construction defines the orientation of every element of the two-complex.

The geometry of B is invariant under both rotations and the time reversal transformation that swaps Σ^p and Σ^f. The discretization reduces the rotational symmetry to a discrete tetrahedral symmetry, realized by an even permutation of the indices a, b, c, d. The time reversal symmetry is realized by the swap of the indices p and f.

There is also a combinatorial symmetry defined by the exchange of the exterior and the interior, namely by the exchange of S_+ and S_-. This is realized in the two-complex by the invariance under the swap of the indices $+$ and $-$. This is however not a symmetry of the geometry we want to study, as S_+ and S_- have a different geometry: S_+ is larger.

III. TRANSITION AMPLITUDE

Following Appendix C, we assign group elements to the edges and the links of the two-complex:

$\mathrm{L}_a^\epsilon \longleftrightarrow h_a^\epsilon \in \mathrm{SU}(2)$;
$\mathrm{L}_{a,b}^{t\epsilon} \longleftrightarrow h_{a,b}^{t\epsilon} \in \mathrm{SU}(2)$;
$\mathrm{E}_a^{t\epsilon} \longleftrightarrow g_a^{t\epsilon} \in \mathrm{SL}(2,\mathbb{C})$;
$\mathrm{E}_{ab}^t \longleftrightarrow g_{ab}^t \in \mathrm{SL}(2,\mathbb{C})$;
$\mathrm{e}_{a,b}^\epsilon \longleftrightarrow g_{a\to b}^\epsilon, g_{a\leftarrow b}^\epsilon \in \mathrm{SL}(2,\mathbb{C})$.

The group element $g_{a\to b}^\epsilon$ is assigned to the oriented half edge of $\mathrm{e}_{a,b}^\epsilon$ having a source in the source of $\mathrm{e}_{a,b}^\epsilon$ and a target in the middle of $\mathrm{e}_{a,b}^\epsilon$. The group element $g_{a\leftarrow b}^\epsilon$ is assigned to the oriented half edge of $\mathrm{e}_{a,b}^\epsilon$ having a source in the target of $\mathrm{e}_{a,b}^\epsilon$ and a target in the middle of $\mathrm{e}_{a,b}^\epsilon$.

It is then straightforward to compute the covariant loop quantum gravity transition amplitude for the black-to-white hole transition by using the expressions reported in Appendix C applied to the two-complex defined above. The two-complex amplitude $W_\mathcal{C}$ expressed in terms of face amplitudes is

$$\begin{aligned} W_\mathcal{C}(h_a^\epsilon, h_{a,b}^{t\epsilon}) = \int_{\mathrm{SL}(2,\mathbb{C})} & \mathrm{d}g_a^{p\epsilon}\mathrm{d}g_{ab}^p\mathrm{d}g_{a\leftrightarrow b}^\epsilon \\ & \times \prod_{a\epsilon} A_a^\epsilon(h_a^\epsilon, g_a^{t\epsilon}) \prod_{ab} A_{a,b}(g_{a\leftrightarrow c}^+, g_{b\leftrightarrow c}^-) \\ & \times \prod_{tab} A_{a,b}^{t+}(h_{a,b}^{t+}, g_a^{t+}, g_{ab}^t, g_{a\leftrightarrow b}^+) \\ & \times \prod_{tab} A_{a,b}^{t-}(h_{a,b}^{t-}, g_a^{t-}, g_{cd}^t, g_{a\leftrightarrow b}^-). \end{aligned} \tag{1}$$

To regularize the expression in (1) we have dropped the integration over one $\mathrm{SL}(2,\mathbb{C})$ element per vertex. We have chosen to drop the integrations over the $g_a^{f\epsilon}$ and g_{ab}^f variables. The integral is independent from these.

To write the face amplitudes we use the following notation. We introduce the $(2j+1)\times(2j+1)$ matrix $\mathcal{D}_\gamma^{(j)}(g)$, $g \in \mathrm{SL}(2,\mathbb{C})$, with matrix elements

$$(\mathcal{D}_\gamma^{(j)}(g))_{mn} \equiv \mathcal{D}_{jmjn}^{(\gamma j,j)}(g), \tag{2}$$

where $\mathcal{D}_{jmj'n}^{(p,k)}$ are the matrix elements of the (p,k) unitary representation of the principal series of $\mathrm{SL}(2,\mathbb{C})$ in the canonical basis that diagonalize the operators L^2 and L_z of the SU(2) subgroup [26]. The matrix $\mathcal{D}_\gamma^{(j)}(g)$ should not be confused with the SU(2) Wigner matrix $D^{(j)}(h)$ with matrix elements $D_{mn}^{(j)}(h)$, $h \in \mathrm{SU}(2)$. Using these, we have

$$A_a^\epsilon(h_a^\epsilon, g_a^{t\epsilon}) = \sum_j d_j \,\mathrm{Tr}[\mathcal{D}_\gamma^{(j)}((g_a^{f\epsilon})^{-1} g_a^{p\epsilon}) D^{(j)}(h_a^\epsilon)], \tag{3}$$

$$
\begin{aligned}
&A_{a,b}(g^{+}_{a\longleftrightarrow c}, g^{-}_{b\longleftrightarrow c}) \\
&\quad \overset{c<d}{=} \sum_j d_j \,\mathrm{Tr}[\mathcal{D}^{(j)}_\gamma((g^{+}_{a\to d})^{-1} g^{+}_{a\to c}) \\
&\qquad \times \mathcal{D}^{(j)}_\gamma((g^{+}_{a\leftarrow c})^{-1} g^{-}_{b\leftarrow d}) \mathcal{D}^{(j)}_\gamma((g^{-}_{b\to d})^{-1} g^{-}_{b\to c}) \\
&\qquad \times \mathcal{D}^{(j)}_\gamma((g^{-}_{b\leftarrow c})^{-1} g^{+}_{a\leftarrow d})],
\end{aligned} \tag{4}
$$

$$
\begin{aligned}
A^{t+}_{a,b}(h^{t+}_{a,b}, g^{t+}_{a}, g^{t}_{ab}, g^{+}_{a\leftrightarrow b}) = \sum_j d_j \,\mathrm{Tr}[\mathcal{D}^{(j)}_\gamma((g^{t+}_{a})^{-1} g^{+}_{a\to b}) \\
\times \mathcal{D}^{(j)}_\gamma((g^{+}_{a\leftarrow b})^{-1} g^{t}_{ab}) D^{(j)}(h^{t+}_{a,b})],
\end{aligned} \tag{5}
$$

$$
\begin{aligned}
A^{t-}_{a,b}(h^{t-}_{a,b}, g^{t-}_{a}, g^{t}_{cd}, g^{-}_{a\leftrightarrow b}) = \sum_j d_j \,\mathrm{Tr}[\mathcal{D}^{(j)}_\gamma((g^{t-}_{a})^{-1} g^{-}_{a\to b}) \\
\times \mathcal{D}^{(j)}_\gamma((g^{-}_{a\leftarrow b})^{-1} g^{t}_{cd}) D^{(j)}(h^{t-}_{a,b})].
\end{aligned} \tag{6}
$$

The transition amplitude for the black-to-white hole transition is then given by

$$
\begin{aligned}
\langle W_{\mathcal{C}} | \psi_{\mathrm{BW}} \rangle = \int_{\mathrm{SU}(2)} \mathrm{d}h^{\epsilon}_{a} \mathrm{d}h^{t\epsilon}_{a,b} \\
\times W_{\mathcal{C}}(h^{\epsilon}_{a}, h^{t\epsilon}_{a,b}) \psi_{\mathrm{BW}}(h^{\epsilon}_{a}, h^{t\epsilon}_{a,b}),
\end{aligned} \tag{7}
$$

where $|\psi_{\mathrm{BW}}\rangle \in \mathcal{H}_\Gamma$ is the extrinsic coherent state peaked on the classical boundary geometry of the black-to-white hole transition that was constructed in [15].

For numerical calculations [27–30] and to use asymptotic techniques [31–33] it is more convenient to use the amplitude written in terms of vertex amplitudes.

Following the notation in Appendix C, we assign a spin [an SU(2) irreducible representation] to every face in the two-complex and an intertwiner, namely a basis element in the space (each edge of the two-complex belongs to four faces)

$$
H_{j_1 \cdots j_4} = \mathrm{Inv}_{\mathrm{SU}(2)}[H_{j_1} \otimes \cdots \otimes H_{j_4}], \tag{8}
$$

to every edge of the two-complex:

$\mathrm{F}^{\epsilon}_{a} \longleftrightarrow J^{\epsilon}_{a} \in \mathbb{N}/2$;
$\mathrm{F}^{t\epsilon}_{a,b} \longleftrightarrow J^{t\epsilon}_{a,b} \in \mathbb{N}/2$;
$\mathrm{f}_{a,b} \longleftrightarrow j_{a,b} \in \mathbb{N}/2$;
$\mathrm{E}^{t\epsilon}_{a} \longleftrightarrow I^{t\epsilon}_{a} \in H_{J^{\epsilon}_{a} J^{t\epsilon}_{a,b}}$;
$\mathrm{E}^{t}_{ab} \longleftrightarrow I^{t}_{ab} \in H_{J^{t+}_{a,b} J^{t-}_{c,d}}$;
$\mathrm{e}^{+}_{a,b} \longleftrightarrow i^{+}_{a,b} \in H_{j_{a,c} J^{t+}_{a,b}}$;
$\mathrm{e}^{-}_{a,b} \longleftrightarrow i^{-}_{a,b} \in H_{j_{c,a} J^{t-}_{a,b}}$.

Using this we can write the two-complex transition amplitude in the following form:

$$
\begin{aligned}
W_{\mathcal{C}}(h^{\epsilon}_{a}, h^{t\epsilon}_{a,b}) = \sum_{J^{\epsilon}_{a} J^{t\epsilon}_{a,b}} \sum_{I^{t\epsilon}_{a} I^{t}_{ab}} \left[\prod_{\epsilon a} d_{J^{\epsilon}_{a}} \prod_{t\epsilon ab} d_{J^{t\epsilon}_{a,b}} \right] \\
\times \left\langle \bigotimes_{t\epsilon a} I^{t\epsilon}_{a} \bigotimes_{ta, b>a} I^{t}_{ab} \middle| \bigotimes_{\epsilon a} D^{(J^{\epsilon}_{a})}(h^{\epsilon}_{a}) \bigotimes_{t\epsilon ab} D^{(J^{t\epsilon}_{a,b})}(h^{t\epsilon}_{a,b}) \right\rangle_{\Gamma} \\
\times W_{\mathcal{C}}(J^{\epsilon}_{a} J^{t\epsilon}_{a,b}, I^{t\epsilon}_{a}, I^{t}_{ab}),
\end{aligned} \tag{9}
$$

where the bra-ket notation indicates the index contraction dictated by Γ [26]. The transition amplitude in the spin-intertwiner basis reads

$$
\begin{aligned}
&W_{\mathcal{C}}(J^{\epsilon}_{a} J^{t\epsilon}_{a,b}, I^{t\epsilon}_{a}, I^{t}_{ab}) \\
&\quad = \sum_{j_{a,b}} \sum_{i^{\epsilon}_{a,b}} \prod_{ab} d_{j_{a,b}} \prod_{\epsilon a} A_{\mathrm{v}^{\epsilon}_{a}}(j_{a,b}, J^{\epsilon}_{a}, J^{t\epsilon}_{a,b}, I^{t\epsilon}_{a}, i^{\epsilon}_{a,b}) \\
&\qquad \times \prod_{a} \prod_{b>a} A_{\mathrm{v}_{ab}}(j_{a,c}, j_{b,c}, J^{t+}_{a,b}, J^{t-}_{c,d}, I^{t}_{ab}, i^{+}_{a,b}, i^{-}_{c,d}).
\end{aligned} \tag{10}
$$

The graphical representation of the product of the vertex amplitudes [whose analytical expression can be easily read from Eq. (C16)] written using the graphical representation of [31,34] can be found in Fig. 2.

Notice the relative simplicity of the expression in Eq. (10). There are only two kinds of local vertex amplitudes (see also Fig. 2): the amplitude associated to the eight five-valent vertices $\mathrm{v}^{\epsilon}_{a}$ and the amplitude associated to the six six-valent vertices v_{ab}.

For example, the amplitude of the five-valent vertex v^{+}_{1} depends on the following quantities. Two "vertical"

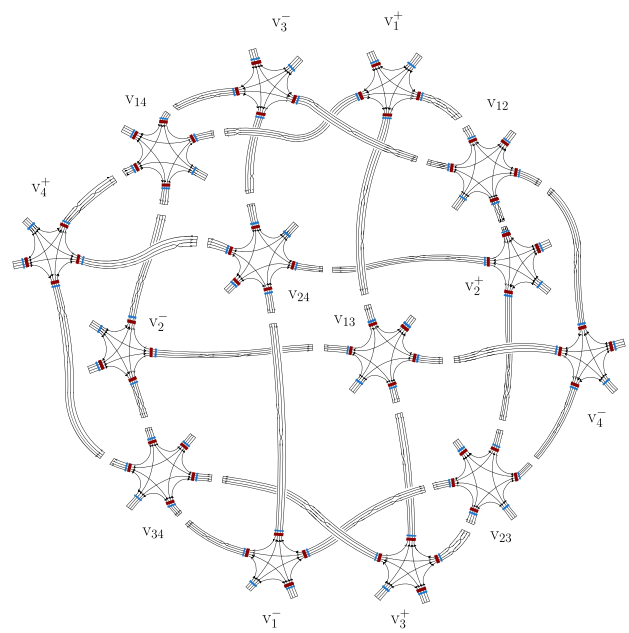

FIG. 2. Graphical representation of the product of the local vertex amplitudes entering the two-complex spin-intertwiner transition amplitude in Eq. (10).

(see Appendix B) boundary intertwiners, the past one I_1^{p+} and the future one I_1^{f+}, and three "horizontal" internal intertwiners $i_{1,2}^+, i_{1,3}^+, i_{1,4}^+$. One vertical spin J_1^+, three vertical past spins $J_{1,2}^p, J_{1,3}^p, J_{1,4}^p$, three vertical future spins $J_{1,2}^f, J_{1,3}^f, J_{1,4}^f$ and finally three spins $j_{1,2}, j_{1,3}, j_{1,4}$ of the horizontal internal faces.

Similarly, the amplitude of the six-valent vertex v_{12} depends on the following quantities: two vertical boundary intertwiners I_{12}^p and I_{12}^f and four horizontal internal intertwiners $i_{1,2}^+, i_{2,1}^+, i_{3,4}^-, i_{4,3}^-$; four vertical past spins $J_{1,2}^{p+}, J_{2,1}^{p+}, J_{3,4}^{p-}, J_{4,3}^{p-}$, four vertical future spins $J_{1,2}^{f+}, J_{2,1}^{f+}$, $J_{3,4}^{f-}, J_{4,3}^{f-}$ and four spins $j_{1,3}, j_{1,4}, j_{2,3}, j_{2,4}$ of the horizontal internal faces.

IV. USING THE SYMMETRY

Focusing on the transition amplitude in the spin-intertwiner basis in Eq. (10), a simplification of the model can be obtained by restricting the computation to spin foam configurations whose coloring respects the geometric symmetries of the problem at hand. Namely, we can simplify the amplitude by performing a symmetry reduction of the model.

In this scenario the boundary spins are fixed to just four independent ones,

$$J_a^\epsilon = \tilde{J}_\epsilon \quad \text{and} \quad J_{a,b}^{t\epsilon} = J_\epsilon, \tag{11}$$

and the boundary intertwiners are fixed to just three independent ones,

$$I_a^{t\epsilon} = I_\epsilon \quad \text{and} \quad I_{a,b}^t = I. \tag{12}$$

Furthermore, simple geometry shows that the symmetry of the tetrahedra dual to the exterior and the interior nodes $\mathrm{N}_a^{t\epsilon}$ (see Appendix A) implies that their geometry is fully determined by the area of their faces [15]. Hence, the two boundary intertwiners I_ϵ are actually uniquely determined by the spins: $I_\epsilon = I_\epsilon(\tilde{J}_\epsilon, J_\epsilon)$. Finally, the symmetric truncation of the model is obtained by restricting to symmetric spin foam configurations, that is

$$j_{a,b} = j \quad \text{and} \quad i_{a,b}^\epsilon = i_\epsilon. \tag{13}$$

The transition amplitude in the spin-intertwiner basis of the symmetry reduced model is then given by

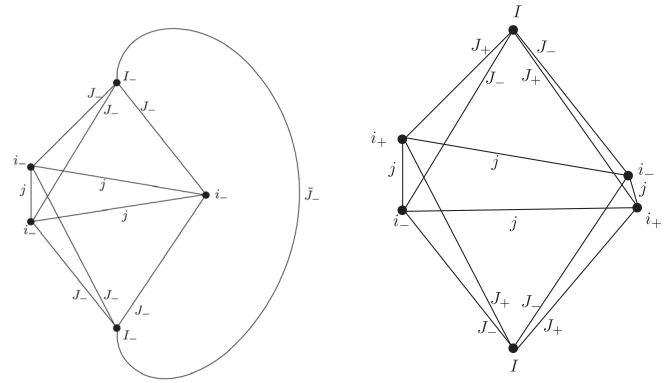

FIG. 3. The boundary graph [26] of the interior five-valent vertices (left) and of the six-valent vertices (right) in the symmetry reduced model.

$$W_{\mathcal{C}}(J_\epsilon, \tilde{J}_\epsilon, I) = \sum_{j, i_\epsilon} d_j^{12} A^6(j, J_\epsilon, I, i_\epsilon) \times \prod_\epsilon A_\epsilon^4(j, J_\epsilon, \tilde{J}_\epsilon, i_\epsilon), \tag{14}$$

where $A(j, J_\epsilon, I, i_\epsilon)$ is the local vertex amplitude associated to every v_{ab} vertex and $A_\epsilon(j, J_\epsilon, \tilde{J}_\epsilon, i_\epsilon)$ is the local vertex amplitude associated to every v_a^ϵ vertex. This is a huge simplification with respect to the transition amplitude in Eq. (10).

The explicit dependence of the vertex amplitudes on the spins and the intertwiners can be read from Fig. 3 or from Fig. 2.

V. COHERENT STATE BASIS

Finally, we give also the expression of the transition amplitude in the overcomplete basis on the intertwiner spaces formed by the coherent intertwiners. This form of the amplitude is useful to study the intrinsic quantum geometry of the cellular complex dual to the two-complex.

Following again the notation in Appendix C, we assign a normal to every couple (edge, face) in the two-complex:

$(\mathrm{E}_a^{t\epsilon}, \mathrm{F}_a^\epsilon) \longleftrightarrow \vec{N}_a^{t\epsilon} \in S^2$;
$(\mathrm{E}_a^{t\epsilon}, \mathrm{F}_{a,b}^{t\epsilon}) \longleftrightarrow \vec{N}_{a,b}^{t\epsilon} \in S^2$;
$(\mathrm{E}_{ab}^t, \mathrm{F}_{a,b}^{t+}) \longleftrightarrow \vec{N}_{ab,a}^{t+} \in S^2$;
$(\mathrm{E}_{ab}^t, \mathrm{F}_{c,d}^{t-}) \longleftrightarrow \vec{N}_{ab,c}^{t-} \in S^2$;
$(\mathrm{e}_{a,b}^\epsilon, \mathrm{F}_{a,b}^{t\epsilon}) \longleftrightarrow \vec{n}_{a,b}^{t\epsilon} \in S^2$;
$(\mathrm{e}_{a,b}^+, \mathrm{f}_{a,c}) \longleftrightarrow \vec{n}_{a,b,c}^+ \in S^2$;
$(\mathrm{e}_{a,b}^-, \mathrm{f}_{c,a}) \longleftrightarrow \vec{n}_{a,b,c}^- \in S^2$.

The change of basis gives

$$W_{\mathcal{C}}(h_a^\epsilon, h_{a,b}^{t\epsilon}) = \sum_{J_a^\epsilon J_{a,b}^{t\epsilon}} \left[\prod_{\epsilon a} d_{J_a^\epsilon} \prod_{t\epsilon ab} d_{J_{a,b}^{t\epsilon}}\right] \int_{S^2} \left(\mathrm{d}^2\vec{N}_a^{t\epsilon} \frac{d_{J_a^\epsilon}}{4\pi}\right)\left(\mathrm{d}^2\vec{N}_{ab,a}^{t+} \frac{d_{J_{a,b}^{t+}}}{4\pi}\right)\left(\mathrm{d}^2\vec{N}_{ab,c}^{t-} \frac{d_{J_{c,d}^{t-}}}{4\pi}\right)\left(\mathrm{d}^2\vec{N}_{a,b}^{t\epsilon} \frac{d_{J_{a,b}^{t\epsilon}}}{4\pi}\right)$$
$$\times \prod_{\epsilon a} \langle J_a^\epsilon, \vec{N}_a^{p\epsilon} D^{(J_a^\epsilon)}(h_a^\epsilon) | J_a^\epsilon, \vec{N}_a^{f\epsilon}\rangle \prod_{tab} \langle J_{a,b}^{t+}, \vec{N}_{ab,a}^{t+} | D^{(J_{a,b}^{t+})}(h_{a,b}^{t+}) | J_{a,b}^{t+}, \vec{N}_{a,b}^{t+}\rangle$$
$$\times \prod_{tab} \langle J_{a,b}^{t-}, \vec{N}_{cd,a}^{t-} | D^{(J_{a,b}^{t-})}(h_{a,b}^{t-}) | J_{a,b}^{t-}, \vec{N}_{a,b}^{t-}\rangle W_{\mathcal{C}}(J_a^\epsilon J_{a,b}^{t\epsilon}, \vec{N}_a^{t\epsilon}, \vec{N}_{ab,a}^{t+}, \vec{N}_{ab,c}^{t-}, \vec{N}_{a,b}^{t\epsilon}), \tag{15}$$

where the transition amplitude in the coherent basis reads

$$W_{\mathcal{C}}(J_a^\epsilon, J_{a,b}^{t\epsilon}, \vec{N}_a^{t\epsilon}, \vec{N}_{ab,a}^{t+}, \vec{N}_{ab,c}^{t-}, \vec{N}_{a,b}^{t\epsilon}) = \sum_{j_{a,b}} \prod_{ab} d_{j_{a,b}} \int_{S^2} \left(\mathrm{d}^2\vec{n}_{a,b}^{t\epsilon} \frac{d_{J_{a,b}^{t\epsilon}}}{4\pi}\right)\left(\mathrm{d}^2\vec{n}_{a,b,c}^{+} \frac{d_{j_{a,c}}}{4\pi}\right)\left(\mathrm{d}^2\vec{n}_{a,b,c}^{-} \frac{d_{j_{c,a}}}{4\pi}\right)$$
$$\times \prod_{\epsilon a} A_{\mathrm{v}_a^\epsilon}(j_{a,b}, J_a^\epsilon, J_{a,b}^{t\epsilon}, \vec{n}_{a,b}^{t\epsilon}, \vec{n}_{a,b,c}^{\epsilon}, \vec{N}_a^{t\epsilon}, \vec{N}_{a,b}^{t\epsilon})$$
$$\times \prod_a \prod_{b>a} A_{\mathrm{v}_{ab}}(j_{\mathrm{v}_{ab}}, J_{\mathrm{v}_{ab}}, \vec{n}_{\mathrm{v}_{ab}}, \vec{N}_{\mathrm{v}_{ab}}) \tag{16}$$

and the labels $j_{\mathrm{v}_{ab}}, J_{\mathrm{v}_{ab}}, \vec{n}_{\mathrm{v}_{ab}}, \vec{N}_{\mathrm{v}_{ab}}$ stand for the following sets of variables:

$$j_{\mathrm{v}_{ab}} = \{j_{a,c}, j_{b,c}\}, \tag{17a}$$

$$J_{\mathrm{v}_{ab}} = \{J_{a,b}^{t+}, J_{c,d}^{t-}\}, \tag{17b}$$

$$\vec{n}_{\mathrm{v}_{ab}} = \{\vec{n}_{a,b}^{t+}, \vec{n}_{c,d}^{t-}, \vec{n}_{a,b,c}^{+}, \vec{n}_{c,d,a}^{-}\}, \tag{17c}$$

$$\vec{N}_{\mathrm{v}_{ab}} = \{\vec{N}_{ab,a}^{t+}, \vec{N}_{ab,c}^{t-}\}. \tag{17d}$$

The analytical expression of the coherent vertex amplitudes in Eq. (16) is given in Eq. (C10). The contraction pattern between the coherent states and the $\mathcal{D}_\gamma^{(j)}$ matrices in the coherent vertex amplitudes exactly matches the contraction pattern between the intertwiners and the $\mathcal{D}_\gamma^{(j)}$ matrices in the spin-intertwiner vertex amplitudes (it is just a change of basis) and it can therefore be read directly from Fig. 2.

VI. CONCLUDING REMARKS

Starting from the results obtained in [15], we have constructed a two-complex that discretizes the quantum region in which the black hole horizon tunnels from a trapping to an antitrapping horizon and we have explicitly computed the transition amplitude associated to the phenomenon using covariant loop quantum gravity.

The two-complex defined in Sec. II is complicated and the corresponding transition amplitude computed in Sec. III may be difficult to studied analytically. However, the high degree of symmetry of the two-complex should help in the numerical exploration of the transition amplitude. A numerical analysis of the transition amplitude is in progress and it will be reported elsewhere.

Notably, the set of internal faces of the two-complex forms a *bubble*, that is they form together a surface without boundary with the topology of a two-sphere. The presence of a bubble in a two-complex may in principle lead to a divergence in the corresponding transition amplitude [26]. A preliminary counting of integration variables and constraints among those appearing in the large spin limit of (16) appears to suggest that the amplitude is exponentially suppressed for large spins, and therefore convergent. A detailed analysis will be reported elsewhere.

ACKNOWLEDGMENTS

This work was made possible through the support of the FQXi Grant No. FQXi-RFP-1818 and of the ID No. 61466 grant from the John Templeton Foundation, as part of the The Quantum Information Structure of Spacetime (QISS) Project (qiss.fr) [35].

APPENDIX A: THE CELLULAR DECOMPOSITION OF B

The triangulation of the boundary Σ of B was constructed in [15] and it can be summarized as follows.

The surface Σ is formed by a past component Σ^p and a future component Σ^f, joined inside the black hole at the two-sphere S_- and outside the black hole at the two-sphere S_+ (see Fig. 1). A simple triangulation of it is obtained by placing four (equidistant) points p_a^- on S_- and four (equidistant) points p_a^+ on S_+.

The triangulation is then defined by the points p_a^ϵ, the segments s_{ab}^ϵ and $s_{a,b}^t$, the triangles L_a^ϵ and $L_{a,b}^{t\epsilon}$, the tetrahedra $N_a^{t\epsilon}$ and N_{ab}^t, and their boundary relations:

$$\partial s_{ab}^\epsilon = (p_a^\epsilon, p_b^\epsilon), \tag{A1a}$$

$$\partial s_{a,b}^t = (p_a^-, p_b^+)^t; \tag{A1b}$$

$$\partial L_a^\epsilon = (s_{bc}^\epsilon, s_{cd}^\epsilon, s_{db}^\epsilon), \tag{A1c}$$

$$\partial L_{a,b}^{t+} = (s_{cd}^+, s_{a,c}^t, s_{a,d}^t), \tag{A1d}$$

$$\partial L_{a,b}^{t-} = (s_{cd}^-, s_{c,a}^t, s_{d,a}^t); \tag{A1e}$$

$$\partial N_a^{t\epsilon} = (L_{a,b}^{t\epsilon}, L_{a,c}^{t\epsilon}, L_{a,d}^{t\epsilon}, L_a^\epsilon), \tag{A1f}$$

$$\partial N_{ab}^t = (L_{a,b}^{t+}, L_{b,a}^{t+}, L_{c,d}^{t-}, L_{d,c}^{t-}). \tag{A1g}$$

The indices a, b, c, d, t and ϵ follow the rules discussed in Sec. II. Partial graphical representations of this triangulation can be found in Figs. 4 and 5.

The graph Γ dual to the triangulation of Σ, which is formed by nodes (dual to the tetrahedra of the triangulation) connected by links (dual to the triangles of the triangulation), is represented in Fig. 8. Using the same label to denote dual objects, it is straightforward to check that the notation in Eq. (A1) is consistent with the notation given in Sec. II for Γ.

The cellular decomposition of B can then be obtained defining internal two-dimensional surfaces $f_{a,b}$, internal three-dimensional cells $e_{a,b}^\epsilon$, internal four-dimensional cells v_a^ϵ and v_{ab}, and their boundary relations:

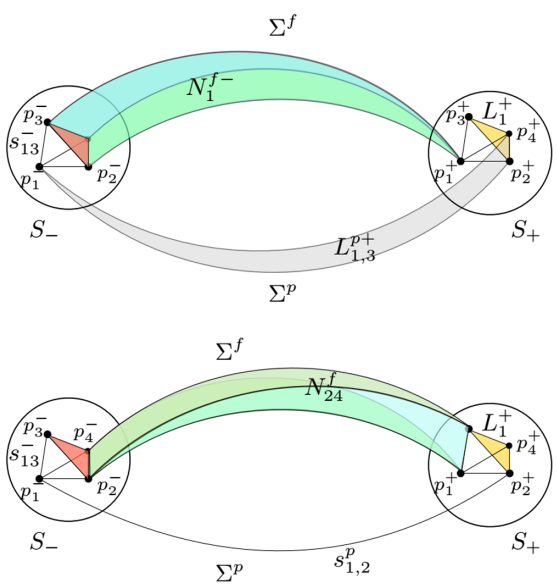

FIG. 4. Elements of the triangulation of Σ seen as embedded objects in the four-dimensional spacetime.

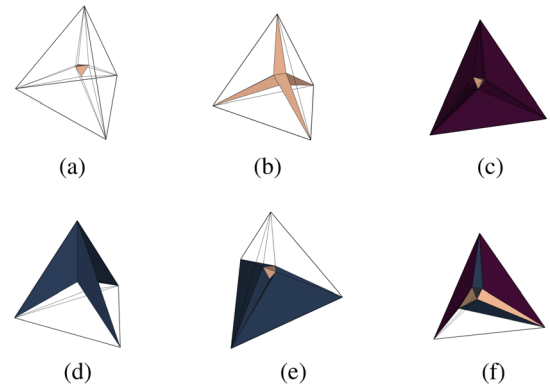

FIG. 5. The triangulation of Σ^t (not Σ) seen as a topological three-dimensional object. Each subfigure has different elements highlighted: in (a) the triangles L_a^- are highlighted; in (b) the four tetrahedra N_a^{t-} are highlighted; in (c) three tetrahedra N_a^{t+} out of four are highlighted; in (d) three tetrahedra N_{ab}^t out of six are highlighted; in (e) the remaining three tetrahedra N_{ab}^t are highlighted; in (f) two tetrahedra N_a^{t-}, two tetrahedra N_a^{t+} and two tetrahedra N_{ab}^t are highlighted.

$$\partial f_{a,b} = (s_{a,b}^p, s_{a,b}^f); \tag{A2a}$$

$$\partial e_{a,b}^\epsilon = (L_{a,b}^{p\epsilon}, L_{a,b}^{f\epsilon}, f_{a,c}, f_{a,d}); \tag{A2b}$$

$$\partial v_a^\epsilon = (N_a^{p\epsilon}, N_a^{f\epsilon}, e_{a,b}^\epsilon, e_{a,c}^\epsilon, e_{a,d}^\epsilon), \tag{A2c}$$

$$\partial v_{ab} = (N_{ab}^p, N_{ab}^f, e_{a,b}^+, e_{b,a}^+, e_{c,d}^-, e_{d,c}^-). \tag{A2d}$$

Notice that the internal two-dimensional surfaces are not triangles, that the internal three-dimensional cells are not tetrahedra and that the internal four-dimensional cells are not four-simplices. The cellular decomposition of B is thus not a four-dimensional triangulation.

The two-complex $\mathcal{C}$, whose combinatorial definition is given in Sec. II, can be equivalently defined (apart from its orientation) as the dual to the cellular decomposition of B specified by Eqs. (A2) and (A1).

APPENDIX B: GRAPHICAL REPRESENTATION OF Γ AND $\mathcal{C}$

The combinatorial characterization of the two-complex given above is complete and compact, but it is difficult to visualize. We give here some graphical representations to help the geometrical intuition.

The graph Γ dual to the triangulation of Σ is depicted in Fig. 6. The lower part of the graph is on Σ^p, the upper is on Σ^f. The left part of the graph, with the four brown nodes N_a^{t-}, is the interior of the black hole; the right part of the graph, with the four red nodes N_a^{t+}, is the exterior of the black hole. The six blue nodes N_{ab}^t are intermediate (they represent tetrahedra cut by the horizon).

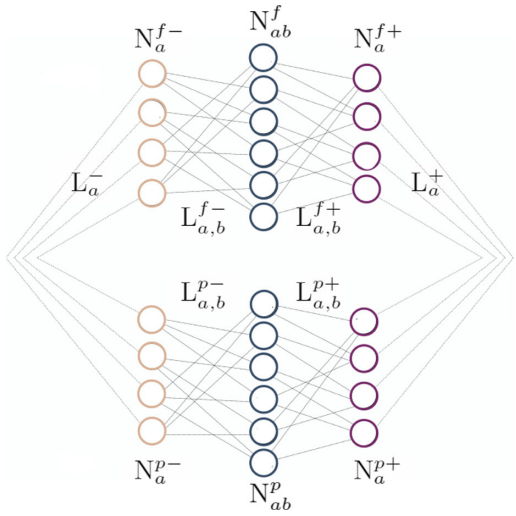

FIG. 6. Two-dimensional representation of the graph Γ dual to the triangulation of Σ.

The structure of the vertices and internal edges of the two-complex reproduces the structure of the past (or future) part of the graph Γ. This is depicted in Fig. 7, using for the vertices the same color codes used for the nodes. The boundary edges are all vertical: they connect the vertices in Fig. 7 with the corresponding past and future nodes in Fig. 6. All the internal faces are horizontal: one of them is depicted in Fig. 7. All the boundary faces are vertical and they are of course in one-to-one correspondence with the links of the graph Γ.

To visualize the faces, it is more convenient to shift to a three-dimensional representation and give up the radial ordering from interior to exterior. The graph Γ can be then represented as in Fig. 8. The upper part of the picture still contains the future objects and the lower part the past objects. The blue dots represent the nodes N_{ab}^{t}, the brown dots represent the nodes N_a^{t-} and the red dots represent the nodes N_a^{t+}, as in Fig. 6, but the interior-middle-exterior order is not respected. The links L_a^{ϵ} vertically connect the nodes $N_a^{p\epsilon}$ in the past to the nodes $N_a^{f\epsilon}$ in the future. The pattern of the links $L_{a,b}^{t\epsilon}$, which is the same on both the past and the future components of the graph, can be better appreciated restricting only to the past (or future) component depicted in Fig. 9.

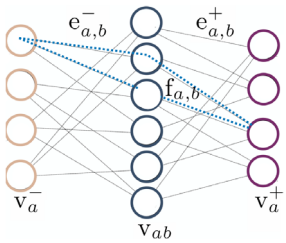

FIG. 7. Two-dimensional representation of the internal component of the two-complex.

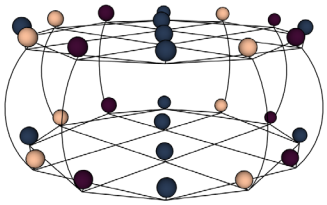

FIG. 8. Three-dimensional representation of the graph Γ dual to the triangulation of Σ; each node is represented as a sphere colored consistently with its dual tetrahedron in Fig. 5.

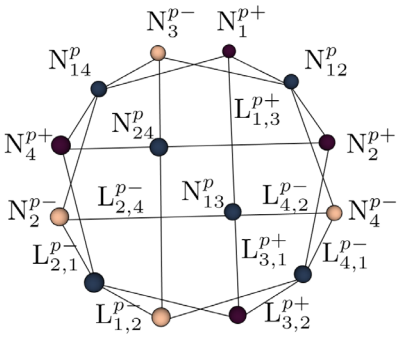

FIG. 9. Two-dimensional representation of the past component of the graph Γ dual to the triangulation of Σ.

The one-skeleton of the two-complex is represented in Fig. 10. Be careful: in Fig. 10 the dots of the upper and lower layers are nodes, while those of the intermediate layer are vertices. The past (lower) and the future (upper) layers are in fact the past and the future components of the boundary graph Γ in Fig. 8. The intermediate layer represents the vertices and the internal edges of the two-complex.

The boundary edges $E_a^{t\epsilon}$ and E_{ab}^{t} can be recognized in Fig. 10 as the edges connecting the internal component of the two-complex to both the past and the future components

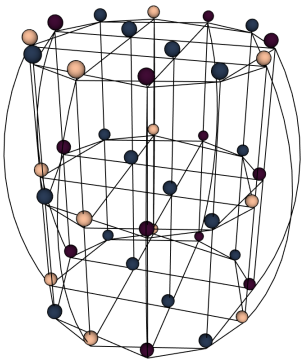

FIG. 10. Three-dimensional representation of the one-skeleton of the two-complex $\mathcal{C}$; notice that although the internal vertices and the boundary nodes are graphically depicted in the same way, they are two very distinct objects (the same applies also to edges and links).

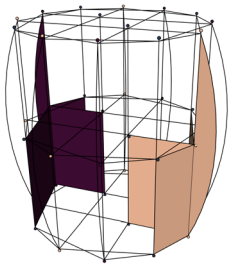

FIG. 11. Graphical representation of the boundary faces (in red) $\mathrm{F}^{p+}_{4,1}$, $\mathrm{F}^{p+}_{4,2}$, $\mathrm{F}^{p+}_{4,3}$, F^{+}_{4} and (in brown) $\mathrm{F}^{p-}_{4,1}$, $\mathrm{F}^{p-}_{4,2}$, $\mathrm{F}^{p-}_{4,3}$, F^{-}_{4}.

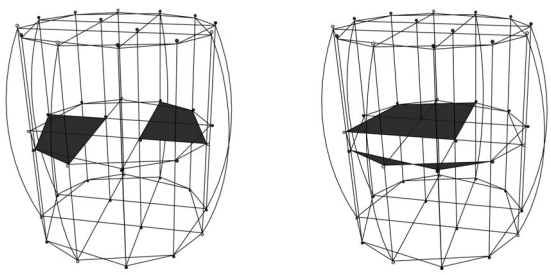

(a) (b)

FIG. 12. Graphical representation of the internal faces $\mathrm{f}_{1,4}$, $\mathrm{f}_{4,1}$ [in (a)] and $\mathrm{f}_{1,2}$, $\mathrm{f}_{3,1}$ [in (b)].

of the boundary. This construction completely specifies the one-skeleton of the two-complex $\mathcal{C}$.

The graphical representation of the boundary faces $\mathrm{F}^{\epsilon}_{a}$ and $\mathrm{F}^{t\epsilon}_{a,b}$ is easily obtained using their definition given in Sec. II. Some of them are depicted in Fig. 11.

The internal faces, although slightly more difficult to represent, can be found in the same way. Some of them are reported in Fig. 12. The strange nature of their graphical representation (some of them intersect each other and some of them have strange shapes) is just a consequence of the fact that we are representing a four-dimensional object in three dimensions and it has no physical meaning.

APPENDIX C: TRANSITION AMPLITUDES IN COVARIANT LOOP QUANTUM GRAVITY

We briefly review how transition amplitudes are expressed in covariant loop quantum gravity focusing on the EPRL-KKL transition amplitudes. For more details, we refer the reader to [26,34,36,37].

Given a compact region of spacetime B with boundary $\Sigma = \partial B$ and an arbitrary oriented graph $\Gamma \in \Sigma$, the boundary Hilbert space of a truncation of the complete quantum theory that considers only the degrees of freedom coming from Γ is $H_\Gamma = L^2[\mathrm{SU}(2)^L/\mathrm{SU}(2)^N]_\Gamma$, where L and N are respectively the total number of links and nodes in Γ. A boundary state, i.e., an element of the boundary space, is a square integrable function $\psi(h_\ell)$ that is gauge invariant at every node $\mathrm{n} \in \Gamma$. Each $h_\ell \in \mathrm{SU}(2)$ can be seen as the holonomy of the Ashtekar-Barbero connection between two nodes of Γ.

A transition amplitude associated to each state in the boundary Hilbert space can then be given in terms of an arbitrary oriented two-complex C whose boundary graph is Γ. Let f, e, v $\in C$ denote respectively a face, an edge and a vertex of C. To each internal edge e linking two vertices v and v′ are assigned two $\mathrm{SL}(2,\mathbb{C})$ elements $g_{ve} = g_{ev}^{-1}$ and $g_{\mathrm{ev}'} = g_{\mathrm{v}'\mathrm{e}}^{-1}$. To each boundary edge E, edges that link an internal vertex v and a node n is assigned one $\mathrm{SL}(2,\mathbb{C})$ element $g_{\mathrm{vn}} = g_{\mathrm{nv}}^{-1}$.

An internal face is denoted as $\mathrm{f} \in B$ and a boundary face, a face that contains a link, is denoted as $\mathrm{F} \in \Gamma$. Given an arbitrary boundary state $|\psi\rangle \in H_\Gamma$, the theory associate to it the amplitude

$$\langle W_C|\psi\rangle = \int_{\mathrm{SU}(2)} \mathrm{d}h_\ell W_C(h_\ell)\psi(h_\ell), \tag{C1}$$

where the two-complex amplitude $W_C(h_\ell)$ is defined as (neglecting the normalization constant)

$$W_C(h_\ell) = \int_{\mathrm{SU}(2)} \mathrm{d}h_{\mathrm{fv}} \prod_{\mathrm{f}\in C} \delta\left(\prod_{\mathrm{v}\in\mathrm{f}} h_{\mathrm{fv}}\right) \prod_{\mathrm{v}\in C} A_{\mathrm{v}}(h_{\mathrm{fv}}). \tag{C2}$$

The vertex amplitude $A_{\mathrm{v}}(h_{\mathrm{fv}})$ is given by

$$A_{\mathrm{v}}(h_{\mathrm{fv}}) = \sum_{j_{\mathrm{f}}} \int_{\mathrm{SL}(2,\mathbb{C})} \mathrm{d}g'_{\mathrm{ve}} \times \prod_{\mathrm{f}\ni\mathrm{v}} [d_{j_{\mathrm{f}}} \mathrm{Tr}(\mathcal{D}^{(j_{\mathrm{f}})}_{\gamma}(g_{\mathrm{e}'_{\mathrm{f}}\mathrm{v}} g_{\mathrm{ve}_{\mathrm{f}}}) D^{(j_{\mathrm{f}})}(h_{\mathrm{fv}}))]. \tag{C3}$$

The prime on $\mathrm{d}g'_{\mathrm{ve}}$ means that, fixing v, the integration is over all possible g_{ev} except one. The edges e_{f} and e'_{f} are the two edges in f that have the vertex v as, respectively, target and source. The matrix $D^{(j)}$ is the Wigner matrix of the d_j-dimensional ($d_j = 2j+1$) representation of SU(2) acting on H_j. The matrix $\mathcal{D}^{(j)}_{\gamma}$ is the $d_j \times d_j$ matrix

$$(\mathcal{D}^{(j)}_{\gamma}(g))_{mn} \equiv \mathcal{D}^{(\gamma j, j)}_{jmjn}(g), \qquad g \in \mathrm{SL}(2,\mathbb{C}), \tag{C4}$$

where $\mathcal{D}^{(p,k)}_{jmj'n}$ are the matrix elements of the (p,k) unitary representation of the principal series of $\mathrm{SL}(2,\mathbb{C})$ in the canonical basis that diagonalize the operators L^2 and L_z of the SU(2) subgroup. Finally, γ is the Barbero-Immirzi parameter.

This is the two-complex amplitude expressed in terms of elementary vertex amplitudes. Inserting Eq. (C3) in Eq. (C2) and performing the integrations over h_{fv}, it is possible to express the two-complex amplitude in terms of elementary face amplitudes. The result is

$$W_C(h_\ell) = \int_{\mathrm{SL}(2,\mathbb{C})} \prod_{\mathrm{v}\in C} \mathrm{d}g'_{\mathrm{ve}} \prod_{\mathrm{f}\in B} A_{\mathrm{f}}(g_{\mathrm{ve}}) \times \prod_{\mathrm{F}\in\Gamma} A_{\mathrm{F}}(h_{\ell_{\mathrm{F}}}, g_{\mathrm{ve}}), \tag{C5}$$

where the amplitude of an internal face is

$$A_{\mathrm{f}}(g_{\mathrm{ve}}) = \sum_{j_{\mathrm{f}}} d_{j_{\mathrm{f}}} \mathrm{Tr}[\mathcal{D}_\gamma^{(j_{\mathrm{f}})}(g_{\mathrm{ev}} g_{\mathrm{ve}'}) \times \mathcal{D}_\gamma^{(j_{\mathrm{f}})}(g_{\mathrm{e}'\mathrm{v}'} g_{\mathrm{v}'\mathrm{e}''}) \cdots \mathcal{D}_\gamma^{(j_{\mathrm{f}})}(g_{\mathrm{e}^{(n)}\mathrm{v}^{(n)}} g_{\mathrm{v}^{(n)}\mathrm{e}})], \tag{C6}$$

and the amplitude of a face with one link in the boundary is

$$A_{\mathrm{F}}(h_{\ell_{\mathrm{F}}}, g_{\mathrm{ve}}) = \sum_{j_{\mathrm{F}}} d_{j_{\mathrm{F}}} \mathrm{Tr}[\mathcal{D}_\gamma^{(j_{\mathrm{F}})}(g_{\mathrm{n}_t\mathrm{v}} g_{\mathrm{ve}'}) \times \mathcal{D}_\gamma^{(j_{\mathrm{F}})}(g_{\mathrm{e}'\mathrm{v}'} g_{\mathrm{v}'\mathrm{e}''}) \cdots \mathcal{D}_\gamma^{(j_{\mathrm{F}})}(g_{\mathrm{e}^{(n)}\mathrm{v}^{(n)}} g_{\mathrm{v}^{(n)}\mathrm{n}_s}) \times D^{(j_{\mathrm{F}})}(h_{\ell_{\mathrm{F}}})]. \tag{C7}$$

The quantities n_s and n_t represent the nodes that are, respectively, source and target of the link ℓ. The value of the label (n) in $\mathrm{e}^{(n)}$ and $\mathrm{v}^{(n)}$ is fixed for each face by the topology of C and Γ.

A third way to express the two-complex transition amplitude is the coherent representation in terms of SU(2) coherent states $|j, \vec{n}\rangle \in H_j$. Starting from either Eq. (C2) or Eq. (C5), the two-complex transition amplitude can be expressed in its coherent representation by explicitly performing the traces in terms of coherent states and inserting coherent resolutions of the identity on H_j,

$$\mathbb{1}_j = \frac{d_j}{4\pi} \int_{S^2} \mathrm{d}^2\vec{n} |j, \vec{n}\rangle\langle j, \vec{n}|, \tag{C8}$$

between all the matrices. Rearranging the result in terms of elementary vertex amplitudes the coherent two-complex transition amplitude can be written as

$$W_C(h_\ell) = \sum_{j_{\mathrm{f}}} \prod_{\mathrm{f}\in C} d_{j_{\mathrm{f}}} \prod_{\mathrm{e}\in C} \prod_{\mathrm{f}\ni\mathrm{e}} \left[\int_{S^2} \mathrm{d}^2\vec{n}_{\mathrm{ef}} \frac{d_{j_{\mathrm{f}}}}{4\pi}\right] \times \prod_{\ell\in\Gamma} \langle j_{\mathrm{f}_\ell}, \vec{n}_{\mathrm{E}_{\mathrm{n}_s}\mathrm{f}_\ell} | D^{(j_{\mathrm{f}_\ell})}(h_\ell) | j_{\mathrm{f}_\ell}, \vec{n}_{\mathrm{E}_{\mathrm{n}_t}\mathrm{f}_\ell}\rangle \times \prod_{\mathrm{v}\in C} A_{\mathrm{v}}(j_{\mathrm{f}}, \vec{n}_{\mathrm{ef}}), \tag{C9}$$

where the coherent vertex amplitude is

$$A_{\mathrm{v}}(j_{\mathrm{f}}, \vec{n}_{\mathrm{ef}}) = \int_{\mathrm{SL}(2,\mathbb{C})} \mathrm{d}g'_{\mathrm{ve}} \times \prod_{\mathrm{f}\ni\mathrm{v}} \langle j_{\mathrm{f}}, \vec{n}_{\mathrm{e_f f}} | \mathcal{D}_\gamma^{(j_{\mathrm{f}})}(g_{\mathrm{e_f v}} g_{\mathrm{ve}'_{\mathrm{f}}}) | j_{\mathrm{f}}, \vec{n}_{\mathrm{e}'_{\mathrm{f}}\mathrm{f}}\rangle. \tag{C10}$$

The label E_{n} is used to denote the boundary edge that has the node n in its boundary.

A priori, this construction assigns to each half-edge ev (assuming the same orientation for each face f having e in its boundary) the state

$$\bigotimes_{\mathrm{f}\ni\mathrm{e}} |j_{\mathrm{f}}\rangle, \vec{n}_{\mathrm{ef}} \in \bigotimes_{\mathrm{f}\ni\mathrm{e}} H_{j_{\mathrm{f}}}. \tag{C11}$$

However, due to SU(2) invariance induced on the half-edge ev by the integration over $g_{\mathrm{ev}} \in \mathrm{SL}(2,\mathbb{C})$, the state assigned to ev can be seen as a coherent intertwiner [38],

$$\int_{\mathrm{SU}(2)} \mathrm{d}h \bigotimes_{\mathrm{f}\ni\mathrm{e}} h \triangleright |j_{\mathrm{f}}\rangle, \vec{n}_{\mathrm{ef}} \in \mathrm{Inv}_{\mathrm{SU}(2)}\left[\bigotimes_{\mathrm{f}\ni\mathrm{e}} H_{j_{\mathrm{f}}}\right]. \tag{C12}$$

This suggests a fourth way to express the transition amplitude: instead of using the overcomplete basis of the coherent intertwiners we could use a basis of intertwiners,

$$|i_{\mathrm{e}}\rangle \in \mathrm{Inv}_{\mathrm{SU}(2)}\left[\bigotimes_{\mathrm{f}\ni\mathrm{e}} H_{j_{\mathrm{f}}}\right], \tag{C13}$$

giving the following resolution of the identity:

$$\mathbb{1} = \sum_{i_{\mathrm{e}}} |i_{\mathrm{e}}\rangle\langle i_{\mathrm{e}}|. \tag{C14}$$

The two-complex transition amplitude can be then schematically rewritten as

$$W_C(h_\ell) = \sum_{j_{\mathrm{f}}, i_{\mathrm{e}}} \prod_{\mathrm{f}\in C} d_{j_{\mathrm{f}}} \left\langle \prod_{\mathrm{E}\in C} i_{\mathrm{E}} | \prod_{\ell\in\Gamma} D^{(j_{\mathrm{f}_\ell})}(h_\ell) \right\rangle \times \prod_{\mathrm{v}\in C} A_{\mathrm{v}}(j_{\mathrm{f}}, i_{\mathrm{e}}), \tag{C15}$$

where the spin-intertwiner vertex amplitude is

$$A_{\mathrm{v}}(j_{\mathrm{f}}, i_{\mathrm{e}}) = \int_{\mathrm{SL}(2,\mathbb{C})} \mathrm{d}g'_{\mathrm{ve}} \times \left\langle \prod_{\mathrm{e}\ni\mathrm{v}} i_{\mathrm{e}} | \prod_{\mathrm{f}\ni\mathrm{v}} \mathcal{D}_\gamma^{(j_{\mathrm{f}})}(g_{\mathrm{e_f v}} g_{\mathrm{ve}'_{\mathrm{f}}}) \right\rangle \tag{C16}$$

and the bra-ket notation indicates the index contraction (between the intertwiners and the matrix elements) dictated by the topology of the two-complex.

[1] H. M. Haggard and C. Rovelli, Black to white hole tunneling: An exact classical solution, Int. J. Mod. Phys. A **30**, 1545015 (2015).

[2] L. Modesto, Disappearance of the black hole singularity in loop quantum gravity, Phys. Rev. D **70**, 124009 (2004).

[3] S. Hossenfelder and L. Smolin, Conservative solutions to the black hole information problem, Phys. Rev. D **81**, 064009 (2010).

[4] R. Gambini and J. Pullin, A scenario for black hole evaporation on a quantum geometry, Proc. Sci. FFP14 (**2016**) 038 [arXiv:1408.3050].

[5] J. Olmedo, S. Saini, and P. Singh, From black holes to white holes: A quantum gravitational, symmetric bounce, Classical Quantum Gravity **34**, 225011 (2017).

[6] D. Malafarina, Classical collapse to black holes and quantum bounces: A review, Universe **3**, 48 (2017).

[7] A. Ashtekar, J. Olmedo, and P. Singh, Quantum extension of the Kruskal spacetime, Phys. Rev. D **98**, 126003 (2018).

[8] A. Ashtekar, J. Olmedo, and P. Singh, Quantum transfiguration of Kruskal black holes, Phys. Rev. Lett. **121**, 241301 (2018).

[9] K. E. A. Clements, Black Hole to White Hole Quantum Tunnelling, http://oatd.org/oatd/record?record=handle%5C%3A10012%5C%2F14950.

[10] N. Bodendorfer, F. M. Mele, and J. Münch, Effective quantum extended spacetime of polymer Schwarzschild black hole, Classical Quantum Gravity **36**, 195015 (2019).

[11] G. E. Volovik, From black hole to white hole via the intermediate static state, Mod. Phys. Lett. A **36**, 2150117 (2021).

[12] J. Ben Achour, S. Brahm, S. Mukohyama, and J. P. Uzan, Consistent black-to-white hole bounces from matter collapse, J. Cosmol. Astropart. Phys. 09 (2020) 020.

[13] J. Münch, Effective quantum dust collapse via surface matching, arXiv:gr-qc/2010.13480.

[14] J. G. Kelly, R. Santacruz, and E. Wilson-Ewing, Black hole collapse and bounce in effective loop quantum gravity, Classical Quantum Gravity **38**, 04LT01 (2021).

[15] F. D'Ambrosio, M. Christodoulou, P. Martin-Dussaud, C. Rovelli, and F. Soltani, End of a black hole's evaporation, Phys. Rev. D **103**, 106014 (2021).

[16] C. Rovelli and F. Vidotto, Planck stars, Int. J. Mod. Phys. D **23**, 1442026 (2014).

[17] H. M. Haggard and C. Rovelli, Quantum-gravity effects outside the horizon spark black to white hole tunneling, Phys. Rev. D **92**, 104020 (2015).

[18] H. M. Haggard and C. Rovelli, Quantum gravity effects around Sagittarius A*, Int. J. Mod. Phys. D **25**, 1644021 (2016).

[19] T. De Lorenzo and A. Perez, Improved black hole fireworks: Asymmetric black-hole-to-white-hole tunneling scenario, Phys. Rev. D **93**, 124018 (2016).

[20] M. Christodoulou, C. Rovelli, S. Speziale, and I. Vilensky, Planck star tunneling time: An astrophysically relevant observable from background-free quantum gravity, Phys. Rev. D **94**, 084035 (2016).

[21] P. Martin-Dussaud and C. Rovelli, Interior metric and ray-tracing map in the firework black-to-white hole transition, Classical Quantum Gravity **35**, 147002 (2018).

[22] F. D'Ambrosio and C. Rovelli, How information crosses Schwarzschild's central singularity, Classical Quantum Gravity **35**, 215010 (2018).

[23] M. Christodoulou and F. D'Ambrosio, Characteristic time scales for the geometry transition of a black hole to a white hole from spin foams, arXiv:1801.03027.

[24] E. Bianchi, M. Christodoulou, F. D'Ambrosio, H. M. Haggard, and C. Rovelli, White holes as remnants: A surprising scenario for the end of a black hole, Classical Quantum Gravity **35**, 225003 (2018).

[25] P. Martin-Dussaud and C. Rovelli, Evaporating black-to-white hole, Classical Quantum Gravity **36**, 245002 (2019).

[26] C. Rovelli and F. Vidotto, *Covariant Loop Quantum Gravity* (Cambridge University Press, Cambridge, England, 2015).

[27] P. Donà and G. Sarno, Numerical methods for EPRL spin foam transition amplitudes and Lorentzian recoupling theory, Gen. Relativ. Gravit. **50**, 127 (2018).

[28] P. Donà, M. Fanizza, G. Sarno, and S. Speziale, Numerical study of the Lorentzian Engle-Pereira-Rovelli-Livine spin foam amplitude, Phys. Rev. D **100**, 106003 (2019).

[29] P. Donà, F. Gozzini, and G. Sarno, Searching for classical geometries in spin foam amplitudes: A numerical method, Classical Quantum Gravity **37**, 094002 (2020).

[30] F. Gozzini, A high-performance code for EPRL spin foam amplitudes, arXiv:2107.13952.

[31] S. Speziale, Boosting Wigner's nj-symbols, J. Math. Phys. (N.Y.) **58**, 032501 (2017).

[32] P. Dona and S. Speziale, Asymptotics of lowest unitary SL(2,C) invariants on graphs, Phys. Rev. D **102**, 086016 (2020).

[33] P. Dona, M. Fanizza, P. Martin-Dussaud, and S. Speziale, Asymptotics of $SL(2,\mathbb{C})$ coherent invariant tensors, arXiv:2011.13909.

[34] A. Perez, The spin foam approach to quantum gravity, Living Rev. Relativity **16**, 3 (2013).

[35] https://www.qiss.fr/.

[36] W. Kaminski, M. Kisielowski, and J. Lewandowski, Spin-foams for all loop quantum gravity, Classical Quantum Gravity **27**, 095006 (2010).

[37] Y. Ding, M. Han, and C. Rovelli, Generalized spinfoams, Phys. Rev. D **83**, 124020 (2011).

[38] E. R. Livine and S. Speziale, New spinfoam vertex for quantum gravity, Phys. Rev. D **76**, 084028 (2007).